Chemical Physics Letters 674 (2017) 64–70

Contents lists available at ScienceDirect

Chemical Physics Letters

journal homepage: www.elsevier.com/locate/cplett

Research paper

Accessing the structural and thermodynamic properties of ultra-thin layers of C32 adsorbed on a SiO_2 surface

Sebastian E. Gutierrez-Maldonado [a,b], Jose Antonio Garate [a,b], Maria Jose Retamal [c,d], Marcelo A. Cisternas [c,d], Ulrich G. Volkmann [c,d], Tomas Perez-Acle [a,b,*]

[a] Computational Biology Lab (DLab), Fundacion Ciencia & Vida, Av. Zañartu 1482, Ñuñoa, Santiago, Chile
[b] Centro Interdisciplinario de Neurociencias de Valparaíso (CINV), Pasaje Harrington 287, Playa Ancha, Valparaíso, Chile
[c] Laboratorio de Superficies (SurfLab), Instituto de Física, Pontificia Universidad Católica de Chile, Av. Vicuña Mackenna 4860, Macul, Santiago, Chile
[d] Centro de Investigación en Nanotecnología y Materiales Avanzados (CIEN-UC), Pontificia Universidad Católica de Chile, Av. Vicuña Mackenna 4860, Macul, Santiago, Chile

ARTICLE INFO

Article history:
Received 19 October 2016
In final form 29 January 2017
Available online 1 February 2017

ABSTRACT

Medium-chain alkanes are important molecules with applications in biology and industry. Notably, their structural properties are scarcely understood. To assess structural and thermodynamic properties of dotriacontane (C32) molecules adsorbed on a SiO_2 surface, we conducted all-atom molecular dynamics (MD) simulations. By analyzing potentials of mean force, order parameters and self-diffusion, we compared the stability and preferential orientation between ordered and disordered systems. Our data confirm the presence of one parallel layer of C32 followed by a mixture of disordered C32 segments exhibiting no thermodynamic preference. This semi-ordered structural model shed light to the interactions between C32 and a SiO_2 surface.

1. Introduction

Medium-chain alkanes are the main constituents of several molecules with biological and industrial relevance. They are important for biosensing and bio-remediation of fossil fuels [1], as microlubricants, anticorrosive agents, and surfactants [2]. Consequently, their structural and dynamical properties have been the focus of both experimental and theoretical studies [3–10]. Given their simplicity and due to their role as prototypes for more complex polymers including biologically relevant molecules such as membranes, alkanes have been used to study the behavior of nano-scale materials such as polymeric thin films [11,12]. Using a variety of tools including atomic force microscopy, X-ray diffraction, high-resolution ellipsometry and more recently, molecular dynamics, it is currently accepted that the behavior of alkane thin films is mainly dominated by surface effects [5,10,13–16].

According to experimental evidence published by Volkmann et al. [17,18], the growth of dotriacontane ($C_{32}H_{66}$, C32) thin films, a linear medium-chain alkane, supported on amorphous silica surfaces covered with their native oxide layer (SiO_2) begins with the formation of a bilayer of C32 molecules with their long axis orientated parallel to the surface. On top of this parallel bilayer, a perpendicular layer is formed, i.e., a layer of C32 molecules with their long axis lays perpendicular to the surface. This layer will continue to grow adding as much perpendicular layers, one on top of each other, as more C32 molecules are added to the system, until the formation of mesoparticles is achieved. This mechanism is known as Stranski-Krastanov growth and is commonly accepted as the growth mechanism for medium-sized alkanes supported on inorganic surfaces such as SiO_2 [19–21]. Despite the advancements represented by these studies, fundamental questions remain to be answered regarding the nature of the physicochemical properties governing the interaction between inorganic surfaces and organic molecules. Moreover, shading lights on these questions is a key step to support the development of nanotechnological systems with application in biotechnology [9,12].

A relevant tool to gain insights with atomic resolution on the behavior of molecules is by using a whole spectrum of computer simulation techniques called Molecular Dynamics (MD). MD techniques offer a set of methods suitable to investigate complex interactions between molecules in heterogeneous systems. During the last years, it has emerged as a powerful tool to study diverse phenomena at the atomic scale, ranging from protein folding, structure-function relationships in proteins, to inorganic/biological interactions [9,12]. In particular, several molecular dynamics simulations of alkanes have been previously reported [3,4,6,8,11,13–16,22–26]. Most simulations performed to date have used united

* Corresponding author at: Computational Biology Lab (DLab), Fundacion Ciencia & Vida, Av. Zañartu 1482, Santiago, Region Metropolitana, P.O. 7780272, Chile.
E-mail addresses: sebastian@dlab.cl (S.E. Gutierrez-Maldonado), jgarate@dlab.cl (J.A. Garate), moretama@uc.cl (M.J. Retamal), mncister@uc.cl (M.A. Cisternas), volkmann@fis.puc.cl (U.G. Volkmann), tomas@dlab.cl (T. Perez-Acle).

http://dx.doi.org/10.1016/j.cplett.2017.01.065
0009-2614/

atom models, in which groups of atoms bonded covalently are replaced for pseudo-atoms whose physicochemical properties account for the whole group [4,11]. These approaches allow longer simulation times, saving precious computational power by neglecting high frequency interactions. Unfortunately, these models tend to oversimplify the studied systems in such a way that important microscopic details may be overlooked. For instance, in recent reports of MD simulations of alkanes, all-atom representations were always necessary to accurately reproduce key structural and physicochemical properties of the systems, such as melting [22,24]. Other reports have shown overestimation of certain parameters such as self-diffusion [27,28]. Although all-atom models impose high requirements in terms of computational time, the availability of increased computational power and the constant development of parallel algorithms for molecular dynamics allow, nowadays, the use of these detailed models.

In this work, we aim to get insights on the structural and thermodynamic properties of C32 molecules adsorbed on a SiO_2 surface. To do so, we rely on a set of all-atom MD simulations at room temperature considering two possible ordered scenarios: (i) a parallel arrangement of three C32 layers, and (ii) a single perpendicular C32 layer on top of two parallel C32 layers (Fig. 1). Next, in order to assess the self-organization of these systems, we performed several MD simulations considering three thin films (Fig. 2) and five temperatures ranging from room temperature, below C32's bulk melting point, to below its bulk boiling point. Our results are presented as time-averages of well-known parameters that have been previously applied to the study of alkanes and other molecules [23,29–32] such as density, order parameters, and self-diffusion. Moreover, by computing the potential of mean force, we evaluated the structural preference of all the assessed conformations of C32 adsorbed on SiO_2. Our results confirm the presence of one parallel layer of C32 in close contact with the SiO_2 surface. Above this layer, the simulations revealed a mixture of C32 segments ordered either parallel or perpendicular to the surface exhibiting no thermodynamic preference producing a semi-ordered structure. By comparing our results to physicochemical properties of C32, we validate our model proposing that this semi-ordered structural model could help to the understanding of the structural and thermodynamical properties governing the interactions between C32 and a SiO_2 surface.

2. Methods

2.1. Systems preparation

An amorphous solid SiO_2 surface of dimensions $11 \times 11 \times 2$ nm^3 was built as described elsewhere [33]. The surface has a mean mass density of 2.15 g/cm^3, which is in good agreement with experimental data [34], and a hydroxyl surface density of 0.73 OH/nm^2 on its upper side. For the ordered systems, each parallel layer was composed by 3 rows of 26 C32 molecules in all-trans configuration, in order to cover the whole SiO_2 surface, while the perpendicular layer was built by rotating by 90° one of the rows composing the parallel layer and replicating it 28 times. The parallel-only (PO) system comprised 3 parallel layers of C32 (Fig. 1A and C), while the parallel/perpendicular (PP) system was composed by two parallel layers and one perpendicular layer (Fig. 1B and D) of C32. For the disordered systems, a C32 box was built by equilibrating a single molecule in vacuum using the NAMD 2.7 simulation package [35] and the CHARMM36 force field parameters for lipids [36]. After equilibration, the C32 molecule was replicated using the Packmol software package [37] taking into account the experimental bulk density of C32 (about 0.812 g/cm^3 at room temperature) and the area of the SiO_2 surface. An initial box of 514 C32 molecules was generated and equilibrated following the MD simulation protocol described below. The resulting box was employed to build three systems representing C32 films of dif-

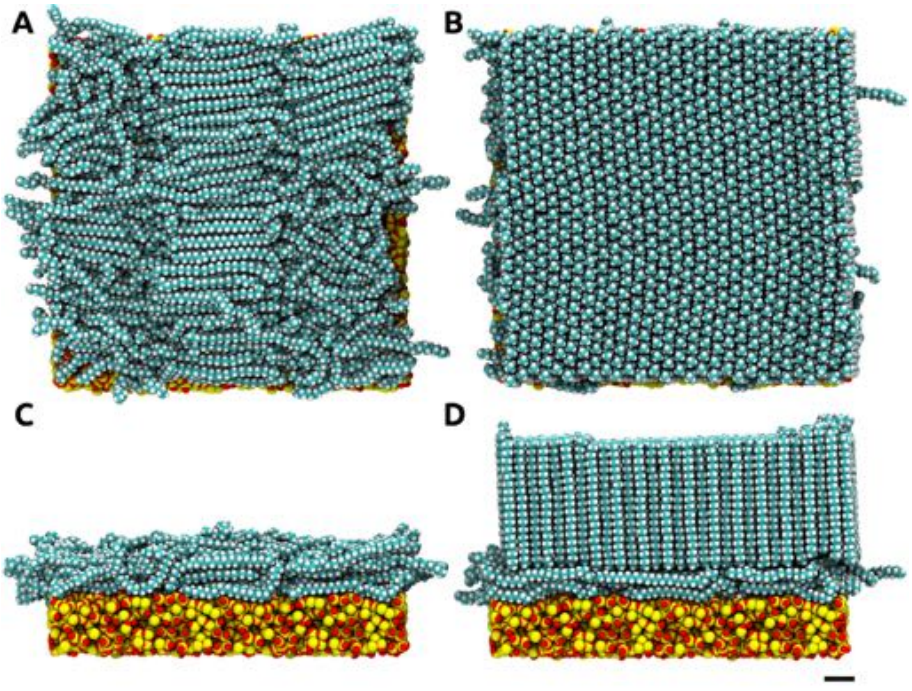

Fig. 1. Representative images of the ordered systems. Top (A and B) and front (C & D) views of both ordered systems. The PO system (A and C) corresponds to a triple parallel layer of C32, whereas the PP system (B and D) corresponds to a double parallel layer with a perpendicular film on top. Both systems are supported on the same SiO_2 surface. Colors correspond to the usual convention: cyan for carbon, white for hydrogen, red for oxygen and yellow for silicon. All molecules are depicted in van der Waals representation. The scale bar corresponds to 10 Å. All images were obtained with the VMD program [43]. (For interpretation of the references to colour in this figure legend, the reader is referred to the web version of this article.)

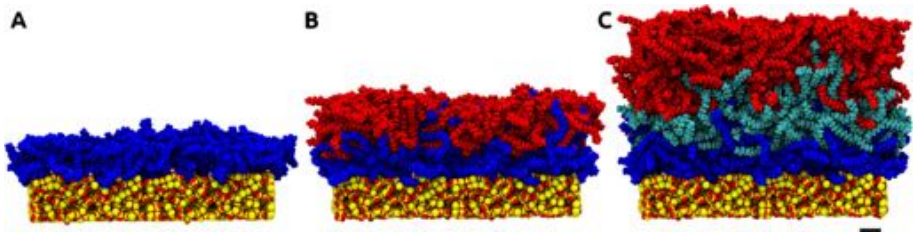

Fig. 2. Representative images of the disordered systems. Disordered systems were built using the 514-C32 system (B) as a starting point (see methods) to produce the 257-C32 system (A) and the 1028-C32 (C). All systems are supported on the same SiO_2 surface. C32 molecules colored in blue, red and cyan correspond to the different layering described for the self-diffusion constants (see main text). Other colors correspond to the usual convention: cyan for carbon, white for hydrogen, red for oxygen and yellow for silicon. All molecules are depicted in van der Waals representation. The scale bar corresponds to 10 Å. All images were obtained with the VMD program [43]. (For interpretation of the references to colour in this figure legend, the reader is referred to the web version of this article.)

ferent thicknesses supported on the SiO_2 surface: a film containing 257 C32 molecules (system 257-C32, Fig. 2A), a film composed of 514 C32 molecules (system 514-C32, Fig. 2B) and a film containing 1028 C32 molecules (system 1028-C32, Fig. 2C). In order to neglect interactions between molecules across the vapor phase, allowing the use of periodic boundary conditions (PBC), the box dimension in the z-direction (normal to the SiO_2 surface) was defined of at least twice the thickness of the corresponding C32 film for each system.

For a detailed description of the simulations and analyzes performed, please refer to the extended supporting methods available online.

3. Results and discussion

We first characterized the ordered systems by using the potential of mean force (PMF) and the order parameters (P_1 & P_2, see methods in ESM file). The PO system shows a well-defined PMF profile, consisting of three basins separated by a 0.2 kcal/mol energy wall between each basin (Fig. 3A, black line). As these PMFs were derived from density, all basins shown in Fig. 2A denote an

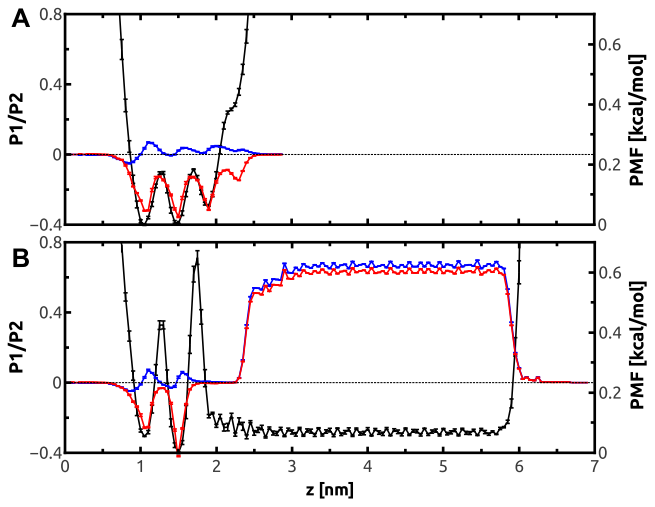

Fig. 3. PMF and order parameter profiles for ordered systems. (A) Profiles for the PO system. (B) Profiles for the PP system. Black lines depict the PMF profiles (right Y axis), while blue and red lines depict P_1 & P_2 profiles (left Y axis), respectively. The x axis represents the height (in nm) of each system, where the origin is located at the geometrical center of the SiO_2 surface. Both PMF profiles show an oscillatory behavior consistent with the internal layering of the ordered systems. Both P_1 & P_2 profiles, up to two nm from the surface, show a parallel ordering for both systems, while showing a perpendicular ordering for the PP system. (For interpretation of the references to colour in this figure legend, the reader is referred to the web version of this article.)

oscillatory behavior that is consistent with the internal layering of the system, as previously reported [23]. Still, as the energy barrier between each basin is lower than thermal fluctuation (~0.5 kcal/mol), no preferential localization for C32 molecules in any of the three layers can be inferred. In the case of the PP system, a similar oscillatory behavior is observed with two well-defined basins that are separated by a 0.4 kcal/mol barrier (Fig. 3B, black line). Notably, a 0.6 kcal/mol energy barrier separates a third broad basin corresponding to the perpendicular layer of this system.

The P_1 profile for the PO system shows an oscillating behavior that fluctuates around zero (Fig. 3A, blue line), reflecting the parallel ordering of the system. On the other hand, the P_1 profile for the PP system shows a similar behavior for the two well-defined basins where C32 molecules orientate parallel to the SiO_2 surface. However, from 2.5 nm and above, P_1 shows a markedly positive profile that co-locates with the broad basin of the PMF corresponding to the perpendicular C32 layer (Fig. 3B, blue line). The P_2 profile complements the information given by P_1, since the negative oscillations seen for both the PO and PP systems correspond to a parallel ordering of the molecules. On the other hand, P_2 positive oscillations seen for the PP system correspond to a perpendicular ordering of the molecules (Fig. 3A and B, red line).

Self-diffusion constants (Table 1) were derived from the MSD of C32 molecules absorbed on SiO_2 (see Section 2). These constants were calculated separately for the parallel and perpendicular layers of both ordered systems (PP and PO). For completeness, whole-layer diffusion (XYZ columns in Table 1) was divided into its two components: in-plane and axial diffusion (XY & Z columns, respectively, Table 1). In terms of whole-layer diffusion, the parallel layer of the PO system diffuses three times faster than the parallel layer of the PP system (0.146×10^{-6} cm^2/s vs 0.050×10^{-6} cm^2/s, respectively). In the case of both systems, in-plane diffusion (XY column, Table 1) resulted an order of magnitude higher than axial diffusion, although the constants for the PO system were still 3-fold greater than that of the PP system. Lower diffusion in the parallel layer of the PP system could be attributed to the confinement produced by the perpendicular layer (see Fig. 1, right panels), which is absent in the PO system, thus allowing free diffusion at the C32/vacuum interface. Self-diffusion of the perpendicular layer is slower than that of the parallel layers of both systems. As expected due to the high symmetry of interactions between alkanes of the perpendicular layer, both in-plane and axial diffusion resulted similar with diffusion values near to 6×10^{-9} cm^2/s.

To better understand whether one conformation is more energetically favorable than the other, either parallel or perpendicular layering, interaction energies were calculated (Table 2). Total internal energy shows an ~8 kcal/mol difference between the parallel and perpendicular ordering, being lower for the latter. As we expected, the conformational energy (i.e., the sum of all bonded terms) of C32 molecules in the perpendicular layer is lower than

Table 1
Self-diffusion constants for the ordered systems.

Systems	Parallel layer			Perpendicular layer		
	XYZ	XY	Z	XYZ	XY	Z
PO	0.146 ± 0.0	0.207 ± 0.0	0.023 ± 0.0	–	–	–
PP	0.050 ± 0.0	0.071 ± 0.0	0.007 ± 0.0	0.006 ± 0.0	0.006 ± 0.0	0.006 ± 0.0

Units in 10^{-6} cm^2/s.

Table 2
Average energy for the ordered systems.

		Electrostatic	Van der Waals	Conformational	Total
Parallel layer	Internal	6.133 ± 0.121	−3.967 ± 0.057	85.940 ± 0.256	88.106 ± 0.392
	Solvation	$-6.953 \times 10^{-4} \pm 5.687 \times 10^{-5}$	$-0.265 \pm 9.237 \times 10^{-3}$	–	$-0.265 \pm 9.256 \times 10^{-3}$
Perpendicular layer	Internal	4.906 ± 0.011	−5.019 ± 0.010	80.795 ± 0.105	80.682 ± 0.111
	Solvation	$-1.924 \times 10^{-3} \pm 1.096 \times 10^{-5}$	$-0.118 \pm 6.888 \times 10^{-5}$	–	$-0.118 \pm 6.713 \times 10^{-5}$

Units in kcal/mol.

that of the parallel layer (Table 2) because the former adopts an all-trans conformation where dihedral angles in the carbon backbone lay at their minimum energy conformation at 180°. Consequently, molecules in the parallel layer would have more degrees of freedom than that of the perpendicular layer due to their localization in the C32/vacuum interface. On the other hand, the difference between solvation energies for both configurations is around 0.1 kcal/mol, thus being equally favorable (Table 2).

From the point of view of interaction energies, both ordered systems would be equally favored and stable. If this is considered to be true, we could expect to see the spontaneous transition from a disordered C32 film into either ordered systems, without preference whatsoever for the PO or the PP arrangement. To test the validity of this hypothesis, we relied on the disordered systems described in methods. On top of this, the effects of two main variables were considered: (i) thickness of the C32 film, and (ii) diffusivity of the system. As described in methods, three disordered systems were produced with 257, 514 and 1028 C32 molecules. Each system was simulated in a range of temperatures from 300 K up to 500 K, using 50 K of increment. Importantly, melting point of C32 is 341 K and boiling point of C32 is 740 K. Therefore, our simulation protocol included one temperature below the melting point (i.e., 300 K) and four temperatures above the melting point but below the boiling point (i.e., 350, 400, 450 and 500 K).

Following the same rationale applied to study the ordered systems, we first analyzed the PMF profiles of the disordered systems at 300 K (Fig. 4, black lines). All three systems show an oscillatory behavior with well-defined basins, similar to what was observed for the PO system (Fig. 3a). As mentioned before, these oscillations have been attributed to a layered deposition of alkane molecules, and their amplitude has been related to the degree of order at the SiO_2/C32 interface [5,23]. However, the amplitude of the oscillations of C32 is small compared to results obtained from other alkanes supported on crystalline surfaces [23], which could imply a less ordered structure (see below). In addition, these oscillations seem to vanish more rapidly as a function of the system's size (see Fig. 4), which has also been observed experimentally and was attributed to the roughness of the substrate [38]. The different energy basins observed in the PMF are separated by walls of ~0.1 kcal/mol, hence no preferential location could be attributed for C32 molecules in these systems. Particularly for the 257-C32 system, the PMF profile is very similar to the one corresponding to the PO system (see Figs. 3A and 4A). In a similar fashion, 2 nm away from the surface and onwards, the 1028-C32 system shows the same behavior than that of the perpendicular layer of the PP system (see Figs. 3B and 4C). Interestingly, the density value associated with this part of the PMF is similar to the experimental bulk density for C32 at room temperature (0.812 g/cm^3, see Fig. S1). As temperature is increased (Figs. S2–4), the location of the two first basins remain roughly the same, while the third basin gradually disappears due to a flattening of the PMF, especially for 514-C32 (Fig. S3, black line) and 1028-C32 (Fig. S4, black line). Also, the energy barrier separating the first and second basins increases

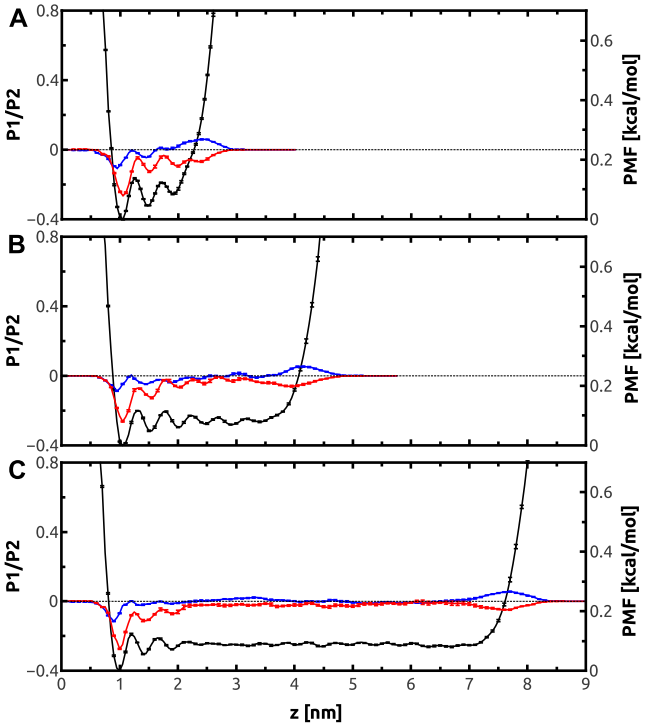

Fig. 4. PMF and order parameter profiles for all disordered systems at 300 K. (A), Profiles for the 257-C32 system. (B), Profiles for the 514-C32 system. (C), Profiles for the 1028-C32 system. Black lines depict the PMF profiles (right Y axis), while blue and red lines depict P_1 & P_2 profiles (left Y axis), respectively. The x axis represents the height (in nm) of each system, where the origin is located at the geometrical center of the SiO_2 surface. PMF profiles for systems 257- & 514-C32 show an oscillatory behavior similar to what was observed for the ordered systems, while for system 1028-C32, oscillations are dampened from 2 nm and onwards. P_1 profile oscillates around zero, except for a small negative peak at 1 nm explained in Supp. Fig. S5. P_2 profile shows a negative peak at 1 nm that co-locates with the first energy basin of the PMF, suggesting the existence of a first parallel layer. (For interpretation of the references to colour in this figure legend, the reader is referred to the web version of this article.)

from its initial value of ~0.1 kcal/mol at 300 K up to ~0.3 kcal/mol at 500 K. The damping of the oscillations as a function of increasing temperature has been observed both theoretically and experimentally for other linear and branched alkanes [8,17,23,38,39].

Both order parameters, P_1 & P_2, show a similar behavior for all three disordered systems: P_1 profiles (Fig. 4, blue lines) have a negative peak close to 1 nm, which indicates a perpendicular orientation that can be justified by some C32 molecules that are trapped inside pockets found on the amorphous surface of the SiO_2 (Fig. S5). Further away from the surface, P_1 values oscillate around zero up to the point where the PMF profiles increase rapidly, meaning either a parallel or bulk-like ordering. P_2 profiles (Fig. 4, red lines) show the same behavior seen for the ordered systems, with a marked negative peak located at the same distance from the surface that co-locates with the first basin of the PMF profile, suggesting that a parallel layer is formed. This negative peak is followed by oscillations in the negative range, which disappear while moving further away from the surface, especially for the 514 & 1028-C32 systems (Fig. 4B and C). In general, these oscillations appear to be sustained until a fixed distance from the surface is reached (about 2.0–2.5 nm), independent of system thickness. From that point onwards, bulk-like order is observed, especially for 1028-C32 system (Fig. 4C). At higher temperatures, both P_1 & P_2 profiles have their first negative peak practically unchanged (see blue and red lines in Figs. S2–S4), while the flattening observed previously occurs closer to the surface (around 1.5 nm). Thus, these distances seems to define a threshold for the influence exerted by the SiO_2 surface that is dependent of the temperature; heating up the systems moves the threshold closer to the surface, probably due to an increase of the thermal energy of the molecules. Other results of similar simulations using an α-quartz surface show only a parallel layer in contact with the surface, since α-quartz surface is flat and isomorph [23]. Importantly, our results also suggest that, independent of the temperature increasing, the first parallel layer of C32 will remain in contact with the SiO_2 surface, denoting a high free energy barrier associated with this layer (Figs. S2–S4). This is an expected behavior considering the industrial applications of C32 as microlubricant.

Altogether, both PMF and order parameters suggest that thin films of C32 near an amorphous SiO_2 surface orientate and pack forming at least one layer parallel with respect to the surface, similar to the first parallel layer observed in the PO system. This layer is present in all three disordered systems and is independent of temperature. Above this layer, entangled C32 segments form a bulk-like phase, which would explain the non-preferential order observed at ~2 nm from the surface onwards.

Self-diffusion constants obtained from the MSD of the disordered systems as a function of the temperature is presented in Table 3. In general terms, 257-C32 has the slower diffusion rates, while 1028-C32 exhibits the fastest ones. Similar whole-system diffusion rates are observed at 300 K among all different systems with values ranging between 0.2–0.3 $\times 10^{-6}$ cm^2/s. Diffusion constants between 257-C32 and 514/1028-C32 differ considerably as temperature increases (especially at 500 K), while diffusion constants for 514-C32 and 1028-C32 are very similar. In-plane diffusion constants are faster than whole-system diffusion at every simulated temperature and, in contrast, axial diffusion constants for all three systems present the slower diffusion rates. In the case of in-plane diffusion constants, although faster than whole-system diffusion rates, a similar behavior is seen in terms of the difference between 257-C32 and 514/1028-C32 (see XY columns, Table 3): at 300 K, all three systems present almost identical diffusion constants with values differing about 10%. These differences are increased at higher temperatures. For axial diffusion constants, there is a drastic variation between 257-C32 and 514/1028-C32: at 300 K, the constant for the former is of 0.050 $\times 10^{-6}$ cm^2/s, while for the latter this value is increased by ~150–200% (see Z columns, Table 3). Unexpectedly, this behavior is maintained roughly across all simulated temperatures.

As axial diffusion varied greatly depending on the thickness of the C32 film, we divided each system in layers along the z axis (colored layers in Fig. 2) to further characterize thickness dependence. Because the average size of each system along the z axis (i.e., their height) increases with temperature, layer definition was fixed in relation to the heights existing at 300 K in order to maintain an unambiguous boundary. To do so, we defined 257-C32 as a one-layered system, because as mentioned before, it is practically identical to the PO system. Using 257-C32 as a reference, we defined 514-C32 as a two-layered system (being roughly twice as thick) and 1028-C32 as a three-layered system (having only one extra layer than the 514-C32). The layer at the SiO_2/C32 interface (bottom-layer, blue molecules in Fig. 2) in both 514/1028-C32 behave similarly, having low diffusion constants, especially for axial diffusion which ranged from 0.034–0.052 $\times 10^{-6}$ cm^2/s (at 300 K) to 0.264–0.273 $\times 10^{-6}$ cm^2/s (at 500 K) (see bottom-layer rows and Z columns in Table S1). Also, in-plane diffusion is higher than axial diffusion, but still lower when compared to the whole film. The layer at the C32/vacuum interface (upper-layer, red molecules in Fig. 2) shows noticeable differences with the bottom-layer, since diffusion rates vary from four- to ten-fold in both 514/1028-C32. In the case of the middle-layer (cyan molecules in Fig. 2), diffusion rates are five- to sixfold higher than for the bottom-layer, and close to 50% of the value for upper-layer diffusion rates.

Considering that C32 intermolecular interaction is the same throughout the system, different diffusion rates observed in our simulations should be explained due to the increasing or decreasing interaction with the SiO_2 surface. In such scenario, we could expect diffusion rates to increase as C32 molecules are farther from the surface, which is indeed the current case as marked differences are observed between bottom-layers and both middle and upper-layers. Moreover, little difference is observed between the middle- and upper-layers for 1028-C32, which might suggest some degree of dampening of the attraction exerted by the SiO_2 surface, either by the bottom-layer or the middle-layer. Since diffusion rates for 514-C32's upper-layer are not so different than that of 1028-C32's middle-layer, there could be a mixed effect in which this layer effectively screens the surface, but still transfers some of the surface's attraction to the upper-layer. This could also

Table 3
Self-diffusion constants for the disordered systems as a function of temperature.

T (K)	257-C32			514-C32			1028-C32		
	XYZ	XY	Z	XYZ	XY	Z	XYZ	XY	Z
300	0.217 ± 0.003	0.301 ± 0.004	0.050 ± 0.000	0.275 ± 0.000	0.334 ± 0.001	0.157 ± 0.000	0.289 ± 0.002	0.324 ± 0.002	0.220 ± 0.001
350	0.571 ± 0.004	0.777 ± 0.005	0.159 ± 0.002	0.756 ± 0.001	0.912 ± 0.002	0.444 ± 0.001	0.853 ± 0.001	0.949 ± 0.002	0.661 ± 0.005
400	1.034 ± 0.004	1.409 ± 0.004	0.286 ± 0.004	1.430 ± 0.003	1.704 ± 0.002	0.884 ± 0.004	1.654 ± 0.002	1.781 ± 0.003	1.400 ± 0.002
450	1.763 ± 0.013	2.380 ± 0.015	0.527 ± 0.010	2.346 ± 0.003	2.772 ± 0.005	1.496 ± 0.010	2.707 ± 0.004	2.957 ± 0.003	2.205 ± 0.006
500	2.530 ± 0.010	3.354 ± 0.006	0.882 ± 0.017	3.686 ± 0.013	4.314 ± 0.009	2.431 ± 0.021	4.061 ± 0.011	4.397 ± 0.008	3.389 ± 0.017

Units in 10^{-6} cm^2/s.

Table 4
Activation energy of self-diffusion for each system.

	257-C32			514-C32			1028-C32		
	XYZ	XY	Z	XYZ	XY	Z	XYZ	XY	Z
Whole film	3.646 ± 0.081	3.591 ± 0.082	4.180 ± 0.147	3.816 ± 0.082	3.760 ± 0.087	4.037 ± 0.066	3.904 ± 0.131	3.851 ± 0.130	4.051 ± 0.149
Upper layer	–	–	–	3.451 ± 0.097	3.411 ± 0.089	3.669 ± 0.201	3.493 ± 0.120	3.440 ± 0.124	3.669 ± 0.123
Middle layer	–	–	–	–	–	–	3.799 ± 0.308	4.230 ± 0.261	0.965 ± 0.260
Bottom layer	–	–	–	3.617 ± 0.192	3.841 ± 0.259	2.463 ± 0.086	3.640 ± 0.293	3.726 ± 0.298	3.127 ± 0.282

Units in kcal/mol.

explain why PMF profiles for 514-C32 and 1028-C32 differ from the bottom-layer and onwards. When comparing these results with the ordered systems, it is clear that 257-C32 behaves as the PO system, although the former has slightly higher diffusion rates than that of the latter. As for the PP system, the bottom-layer of this ordered system has the lowest self-diffusion constants overall, with its axial self-diffusion constant being very similar to the bottom-layers of systems 514- and 1028-C32. As mentioned before, this behavior could be explained by partial confinement produced by the upper and middle layers, respectively.

Temperature dependence of the calculated diffusion constants is properly described by an Arrhenius plot, from which the activation energy of self-diffusion (E_D) can be obtained (Table 4). E_D can be understood as the sum of the energy required to form a void into which the diffusing molecule can move and the energy needed to transfer it from the force field of its nearest neighbors into the void [40]. The obtained energy data reinforces what was already described with the self-diffusion constants: axial diffusion is less favorable than in-plane diffusion, since the activation energy of self-diffusion for the latter is smaller (Table 4). This is observed for all three systems, being more noticeable for 257-C32. When considering each separate layer, a similar behavior is seen for the upper layers compared to the film as a whole: axial diffusion is less favorable than in-plane diffusion. As for the bottom layers, something unexpected is seen for axial diffusion: although rates are slower than for in-plane diffusion (see Table 3), its activation energy is lower, especially for 514-C32 (Table 4). This seems contradictory since lower activation energies should translate into higher diffusion rates. As mentioned earlier, E_D is the sum of two energies: the energy needed to form a void and the energy needed to move a molecule into that void. So, considering that axial diffusion rates are slow, lower activation energies for axial diffusion could be interpreted as one energy term being much higher than the other, while for in-plane diffusion both energy terms could be very similar. Since PMF profiles (Fig. 4) showed practically no energy barriers between consecutive basins, a diffusive process should guide the axial movement of a molecule through the system. Thus, energy needed to form the void should be greater than the energy needed to move a molecule into that void, precluding axial diffusion. Experimental assessment of self-diffusion constants for C32 at different temperatures obtained from nuclear magnetic resonance (NMR) [41] and quasielastic neutron scattering (QENS) experiments [40], shows that our self-diffusions constants are actually 1 or 2 orders of magnitude below such measurements. It is important to note that our self-diffusion rates consider alkanes in close interaction with a SiO_2 surface, which is expected to alter the experimental behavior in terms of diffusion. On the other hand, our estimation of E_D (between 3.64 and 3.90 kcal/mol, see Table 4) is in good agreement with data obtained by QENS (3.87 kcal/mol) [40] as well as with data obtained from other MD simulations with similar time scales (3.91 kcal/mol) [27]. In Smuda et al. [40], it is discussed that NMR and QENS data differ from each other since NMR data covers long-time long-range diffusion (μs to ms), while QENS data covers short-time diffusion (<60 ps). Although our MD simulations span by several nanoseconds length, self-diffusion constants were derived from a ps time scale where we computed the MSD (see Section 2). Therefore, it is expected that E_D obtained from our simulations agree with the one obtained experimentally by QENS.

4. Conclusions

We have performed all-atom molecular dynamics simulations of ordered and disordered thin films of C32 near an amorphous SiO_2 surface considering different temperatures and system sizes. Our results support previous structural conclusions generated from available experimental data [17,34,42] suggesting that, while both ordered systems (PO and PP) could be possible, the perpendicular orientation is more energetically favorable than that of the parallel one. When trying to reach the ordered state from a disordered one, we observe that C32 forms at least one or two parallel layers at the SiO_2/C32 interface. Successive layers of C32 show neither the preferential ordering nor the orientation expected in an ordered model. Instead, a disordered bundle appears from the second parallel layer and above, producing entangled molecular segments that remain at all tested temperatures. As a whole, our results shed lights on the nature of physicochemical properties that govern the interaction between SiO_2 and C32.

Funding

This work was supported by Fundación Ciencia para la Vida Programa de Financiamiento Basal PFB16 (PIA CONICYT), Centro Interdisciplinario de Neurociencia de Valparaiso (ICM-Economia P09-022-F), FONDECYT Postdoc 3160803 (MJR), FONDECYT 1141105 (UV), FONDECYT 1160574 (TPA). SEGM & MC acknowledge a Ph. D scholarship from CONICYT. Supported by the High Performance Computing infrastructure of the NLHPC 'Powered@NLHPC'.

Acknowledgments

SEGM would like to acknowledge Felipe Nuñez & Hector Urbina for their help with calculations and scripts used.

Appendix A. Supplementary material

Supporting Methods describing simulation protocol and analyzes performed. Supporting Fig. S1, Density profile for system 1028-C32 at 300 K. Supporting Figs. S2–S4, PMF and order profiles for the disordered systems at all temperatures above C32's melting point. Supporting Fig. S5, Detail of a C32 molecule trapped in the SiO_2 surface. Supporting Table S1, Self-diffusion constants for each layer of the disordered systems. Supplementary data associated with this article can be found, in the online version, at http://dx.doi.org/10.1016/j.cplett.2017.01.065.

References

[1] T.P. Call, M.K. Akhtar, F. Baganz, C. Grant, Modulating the import of medium-chain alkanes in *E. coli* through tuned expression of FadL, J. Biol. Eng. 10 (2016) 5, http://dx.doi.org/10.1186/s13036-016-0026-3.

[2] A. Iakovlev, D. Bedrov, M. Müller, Alkyl-based surfactants at a liquid mercury surface: computer simulation of structure, self-assembly, and phase behavior, J. Phys. Chem. Lett. 7 (2016) 1546–1553, http://dx.doi.org/10.1021/acs.jpclett.6b00494.

[3] M. Mondello, G.S. Grest, Molecular dynamics of linear and branched alkanes, J. Chem. Phys. 103 (1995) 7156.

[4] T. Shimizu, T. Yamamoto, Melting and crystallization in thin film of n-alkanes: a molecular dynamics simulation, J. Chem. Phys. 113 (2000) 3351.

[5] A. Hashibon, J. Adler, M.W. Finnis, W.D. Kaplan, Ordering at solid-liquid interfaces between dissimilar materials, Interface Sci. 9 (2001) 175.

[6] J.-C. Wang, K.A. Fichthorn, Molecular dynamics studies of the effects of chain branching on the properties of confined alkanes, J. Chem. Phys. 116 (2002) 410, http://dx.doi.org/10.1063/1.1419258.

[7] P. Lang, Surface induced ordering effects in soft condensed matter systems, J. Phys. Condens. Matter 16 (2004) R699, http://dx.doi.org/10.1088/0953-8984/16/23/R02.

[8] K.C. Daoulas, V.A. Harmandaris, V.G. Mavrantzas, Detailed atomistic simulation of a polymer melt/solid interface: structure, density, and conformation of a thin film of polyethylene melt adsorbed on graphite, Macromolecules 38 (2005) 5780, http://dx.doi.org/10.1021/ma050176r.

[9] D. Lu, A. Aksimentiev, A.Y. Shih, E. Cruz-Chu, P.L. Freddolino, A. Arkhipov, K. Schulten, The role of molecular modeling in bionanotechnology, Phys. Biol. 3 (2006) S40, http://dx.doi.org/10.1088/1478-3975/3/1/S05.

[10] W.D. Kaplan, Y. Kauffmann, Structural order in liquids induced by interfaces with crystals, Annu. Rev. Mater. Sci. 36 (2006) 1, http://dx.doi.org/10.1146/annurev.matsci.36.020105.104035.

[11] T. Yamamoto, K. Nozaki, A. Yamaguchi, N. Urakami, Molecular simulation of crystallization in n-alkane ultrathin films: effects of film thickness and substrate attraction, J. Chem. Phys. 127 (2007) 154704, http://dx.doi.org/10.1063/1.2781390.

[12] F. González-Nilo, T. Pérez-Acle, S. Guínez-Molinos, D.A. Geraldo, C. Sandoval, A. Yévenes, L.S. Santos, V.F. Laurie, H. Mendoza, R.E. Cachau, Nanoinformatics: an emerging area of information technology at the intersection of bioinformatics, computational chemistry and nanobiotechnology, Biol. Res. 44 (2011) 43–51, http://dx.doi.org/10.4067/S0716-97602011000100006.

[13] F.Y. Hansen, K.W. Herwig, B. Matthies, H. Taub, Intramolecular and lattice melting in n-alkane monolayers: an analog of melting in lipid bilayers, Phys. Rev. Lett. 83 (1999) 2362.

[14] H. Mo, S. Trogisch, H. Taub, S.N. Ehrlich, U.G. Volkmann, F.Y. Hansen, M. Pino, Studies of the structure and growth mode of dotriacontane films by synchrotron X-ray scattering and molecular dynamics simulations, J. Phys. Condens. Matter 16 (2004) S2905–S2910, http://dx.doi.org/10.1088/0953-8984/16/29/005.

[15] A.D. Enevoldsen, F.Y. Hansen, A. Diama, L. Criswell, H. Taub, Comparative study of normal and branched alkane monolayer films adsorbed on a solid surface. I. Structure, J. Chem. Phys. 126 (2007) 104703, http://dx.doi.org/10.1063/1.2464091.

[16] A. Diama, B. Matthies, K.W. Herwig, F.Y. Hansen, L. Criswell, H. Mo, M. Bai, H. Taub, Structure and phase transitions of monolayers of intermediate-length n-alkanes on graphite studied by neutron diffraction and molecular dynamics simulation, J. Chem. Phys. 131 (2009) 84707, http://dx.doi.org/10.1063/1.3212095.

[17] U.G. Volkmann, M. Pino, L.A. Altamirano, H. Taub, F.Y. Hansen, High-resolution ellipsometric study of an n-alkane film, dotriacontane, adsorbed on a SiO_2 surface, J. Chem. Phys. 116 (2002) 2107, http://dx.doi.org/10.1063/1.1429645.

[18] H. Mo, H. Taub, U.G. Volkmann, M. Pino, S.N. Ehrlich, F.Y. Hansen, E. Lu, P. Miceli, A novel growth mode of alkane films on a SiO_2 surface, Chem. Phys. Lett. 377 (2003) 99, http://dx.doi.org/10.1016/S0009-2614(03)01106-0.

[19] A. Holzwarth, S. Leporatti, H. Riegler, Molecular ordering and domain morphology of molecularly thin triacontane films at SiO_2/air interfaces, Eur. Lett. 52 (2000) 653.

[20] S. Trogisch, M.J. Simpson, H. Taub, U.G. Volkmann, M. Pino, F.Y. Hansen, Atomic force microscopy measurements of topography and friction on dotriacontane films adsorbed on a SiO_2 surface, J. Chem. Phys. 123 (2005) 154703, http://dx.doi.org/10.1063/1.2060707.

[21] M. Bai, K. Knorr, M.J. Simpson, S. Trogisch, H. Taub, S.N. Ehrlich, H. Mo, U.G. Volkmann, F.Y. Hansen, Nanoscale observation of delayering in alkane films, Eur. Lett. 79 (2007) 26003, http://dx.doi.org/10.1209/0295-5075/79/26003.

[22] M.J. Connolly, M.W. Roth, P.A. Gray, C. Wexler, Explicit hydrogen molecular dynamics simulations of hexane deposited onto graphite at various coverages, Langmuir 24 (2008) 3228, http://dx.doi.org/10.1021/la703040a.

[23] M. Tsige, S.S. Patnaik, An all-atom simulation study of the ordering of liquid squalane near a solid surface, Chem. Phys. Lett. 457 (2008) 357, http://dx.doi.org/10.1016/j.cplett.2008.04.026.

[24] L. Firlej, B. Kuchta, M.W. Roth, M.J. Connolly, C. Wexler, Structural and phase properties of tetracosane (C24H50) monolayers adsorbed on graphite: an explicit hydrogen molecular dynamics study, Langmuir 24 (2008) 12392, http://dx.doi.org/10.1021/la802071a.

[25] M.A. Amat, G.C. Rutledge, Liquid-vapor equilibria and interfacial properties of n-alkanes and perfluoroalkanes by molecular simulation, J. Chem. Phys. 132 (2010) 114704, http://dx.doi.org/10.1063/1.3356219.

[26] P. Soza, F.Y. Hansen, H. Taub, M. Kiwi, E. Cisternas, U.G. Volkmann, V. del Campo, Molecular-dynamics simulation of lateral friction in contact-mode atomic force microscopy of alkane films: the role of molecular flexibility, Eur. Lett. 95 (2011) 36001, http://dx.doi.org/10.1209/0295-5075/95/36001.

[27] S.H. Lee, T. Chang, Viscosity and diffusion constants calculation of n-alkanes by molecular dynamics simulations, Bull. Korean Chem. Soc. 24 (2003) 1590–1598, http://dx.doi.org/10.5012/bkcs.2003.24.11.1590.

[28] T. Unruh, C. Smuda, S. Busch, J. Neuhaus, W. Petry, Diffusive motions in liquid medium-chain n-alkanes as seen by quasielastic time-of-flight neutron spectroscopy, J. Chem. Phys. 129 (2008) 121106, http://dx.doi.org/10.1063/1.2990026.

[29] T.K. Xia, J. Ouyang, M.W. Ribarsky, U. Landman, Interfacial alkane films, Phys. Rev. Lett. 69 (1992) 1967.

[30] T.K. Xia, U. Landman, Structure and dynamics of surface crystallization of liquid n-alkanes.pdf, Phys. Rev. B 48 (1993) 11313.

[31] M. Tsige, G.S. Grest, Surface tension and surface orientation of perfluorinated alkanes, J. Phys. Chem. C 112 (2008) 5029.

[32] F. Pierce, M. Tsige, O. Borodin, D. Perahia, G.S. Grest, Interfacial properties of semifluorinated alkane diblock copolymers, J. Chem. Phys 128 (2008) 214903, http://dx.doi.org/10.1063/1.2924120.

[33] E.R. Cruz-Chu, A. Aksimentiev, K. Schulten, Water–silica force field for simulating nanodevices, J. Phys. Chem. B 110 (2006) 21497–21508, http://dx.doi.org/10.1021/jp063896o.

[34] V. del Campo, E. Cisternas, H. Taub, I. Vergara, T. Corrales, P. Soza, U.G. Volkmann, M. Bai, S.-K. Wang, F.Y. Hansen, H. Mo, S.N. Ehrlich, Structure and growth of vapor-deposited n-dotriacontane films studied by X-ray reflectivity, Langmuir 25 (2009) 12962–12967, http://dx.doi.org/10.1021/la901808t.

[35] J.C. Phillips, R. Braun, W. Wang, J. Gumbart, E. Tajkhorshid, E. Villa, C. Chipot, R. D. Skeel, L. Kalé, K. Schulten, Scalable molecular dynamics with NAMD, J. Comput. Chem. 26 (2005) 1781–1802, http://dx.doi.org/10.1002/jcc.20289.

[36] J.B. Klauda, R.M. Venable, J.A. Freites, J.W. O'Connor, D.J. Tobias, C. Mondragon-Ramirez, I. Vorobyov, A.D. MacKerell, R.W. Pastor, Update of the CHARMM all-atom additive force field for lipids: validation on six lipid types, J. Phys. Chem. B 114 (2010) 7830, http://dx.doi.org/10.1021/jp101759q.

[37] L. Martínez, R. Andrade, E.G. Birgin, J.M. Martínez, Software news and update packmol: a package for building initial configurations, J. Comput. Chem. 30 (2009) 2159, http://dx.doi.org/10.1002/jcc.

[38] C.-J. Yu, A.G. Richter, A. Datta, M.K. Durbin, P. Dutta, Observation of molecular layering in thin liquid films using X-ray reflectivity, Phys. Rev. Lett. 82 (1999) 2326, http://dx.doi.org/10.1103/PhysRevLett. 82.2326.

[39] H. Mo, G. Evmenenko, P. Dutta, Ordering of liquid squalane near a solid surface, Chem. Phys. Lett. 415 (2005) 106, http://dx.doi.org/10.1016/j.cplett.2005.08.142.

[40] C. Smuda, S. Busch, G. Gemmecker, T. Unruh, Self-diffusion in molecular liquids: medium-chain n-alkanes and coenzyme Q_{10} studied by quasielastic neutron scattering, J. Chem. Phys. 129 (2008) 14513, http://dx.doi.org/10.1063/1.2943673.

[41] E. von Meerwall, S. Beckman, J. Jang, W.L. Mattice, Diffusion of liquid n-alkanes: free-volume and density effects, J. Chem. Phys. 108 (1998) 4299, http://dx.doi.org/10.1063/1.475829.

[42] S. Basu, S.K. Satija, In-situ X-ray reflectivity study of alkane films grown from the vapor phase, Langmuir 23 (2007) 8331, http://dx.doi.org/10.1021/la062517f.

[43] W. Humphrey, A. Dalke, K. Schulten, VMD - visual molecular dynamics, J. Mol. Graphics 14 (1996) 33–38, http://dx.doi.org/10.1016/0263-7855(96)00018-5.